AD641394

Final Technical Report

Contract NOnr-3942(00)
U. S. Office of Naval Research
ARPA Order No. 125

ELECTRON-TIME OF-FLIGHT SPECTROMETER

G. C. Baldwin, Principal Investigator

Research and Development Center
General Electric Company
Schenectady, New York

October 1, 1966

"Reproduction in whole or in part is permitted for any purpose of the United States Government".

CLEARINGHOUSE
FOR FEDERAL SCIENTIFIC AND
TECHNICAL INFORMATION

Hardcopy	Microfiche		
$3.00	$.50	54 pp	as

ARCHIVE COPY

A Time-Of-Flight Electron Velocity Spectrometer

G. C. BALDWIN AND S. I. FRIEDMAN

Research and Development Center
General Electric Company
Schenectady, New York

---

* Work supported by the Advanced Research Projects Agency thru Contract NOnr-3942(00) issued by the U. S. Office of Naval Research to the Schenectady Tube Operation of the General Electric Company.

"Reproduction in whole or in part is permitted for any purpose of the United States Government".

ABSTRACT

A velocity selector is described which is designed for measurement of the total collision cross section of electrons in the energy region below one volt. The system determines the distributions of times of flight of single electrons over a measured path at selected pressures of a specimen gas. The electrons are generated by repetitive illumination of a photo-emitter by a spark gap, pass over a shielded drift path, enter an accelerating field, and impinge on an electron multiplier. Electronic equipment and data reduction for analysis of time-of-flight and amplitude distributions of electron counts are described; data illustrative of performance are presented, including typical transmission measurements in helium and argon which extend to 100 millivolts. Applications and extensions of the technique are discussed.

CONTENTS

CONTENTS (continued)

I. INTRODUCTION

This paper describes the development and initial performance of an instrumental system intended for measurement of electron-molecule total collision cross sections with velocity-selected electrons in the energy range below 1 eV.

Need exists for detailed electron-molecule interaction data in many fields of pure and applied science, ranging from chemistry to gaseous electronics, energy conversion, and communication.

There are few direct measurements of the electron–molecule cross section in this energy range[1] and these are often discordant.[2-6] Indirect methods using electron swarms apply to much lower energies than have previously been reached in direct, beam-type measurements with velocity-selected electrons, and they do not give the energy dependence of the cross section unambiguously.[7]

Very precise measurements have been reported with electrostatic analyzers,[8] but despite high resolution, it has proved difficult to use these instruments at energies below one volt. Ramsauer and Kollath,[9] employing a magnetic deflection velocity selector, claimed to have reached 0.16 eV, but this claim appears to be negated by the recent work of Golden and Bandel, who found lower limits to this technique at 0.30 eV in helium[10] and at 0.25 in hydrogen.[11] This casts doubt on the accuracy of proposed extrapolations, in which the Ramsauer-Kollath data are fitted to theoretical formulas.[12]

The basic difficulty with velocity selection techniques employing electrostatic or magnetic deflection is the high accuracy with which both the analyzing field and the particle path must be defined. Contact potential irregularities on the bounding electrodes limit the precision of the electrostatic field geometry; for example, Golden and Bandel.[11] observed changes of contact potential amounting to several tenths of a volt between the thermionic electron source and the slits in their Ramsauer-Kollath apparatus. The resulting irregular fields strongly perturb the electron trajectory unless the particle energy is much higher than the differences of contact potential.

The time-of-flight (TOF) method of velocity selection does not require interaction of the particle with the apparatus except at the termini of its path,

nor does it require that the path conform precisely to a chosen geometry (i. e., slight curvature of the trajectory is tolerable). It is inherently less sensitive, therefore, to contact potential differences. It has been widely used with neutrons (for which deflection experiments cannot be performed, but not with electrons, despite the importance of transit-time effects in many electronic devices.

In contrast to deflection techniques, the determination of electron energy by timing flight over a measured distance becomes increasingly precise as the electron energy is reduced. Moreover, the continuous distribution of velocities obtained from conventional electron sources enables measurements to be made simultaneously over an extended energy range, using multichannel registration. Space charge is not a consideration because only a single electron is in transit on any one timing cycle.

II. DESIGN CONSIDERATIONS

2.1 General Concept of the Spectrometer

The General Electric electron TOF velocity selector[13] is basically a photomultiplier with its photo-cathode and first dynode separated by a drift space of about one-half meter into which the specimen gas can be introduced at known concentration. The photoemitter is illuminated periodically with brief flashes of ultraviolet light from a spark gap. An aperture in a surrounding baffle transmits a fraction of the emitted electrons into an elongated magnetically - and electrically - shielded drift space, with a grid at its far extremity. Electrons which reach the grid are accelerated and focused onto a secondary emission multiplier. Bias potentials appropriate for contact potential compensation are applied to each electrode. Multichannel time- and pulse-height analysis of the detector counts allows the electron velocity distribution and the detection efficiency to be inferred. The total electron emission is read with an electrometer. Gases introduced into the flight path will modify these quantities, in a manner which can be related to the energy dependence of the total collision probability in the sample substance.

2.2 Conditions for a Time of Flight Experiment

1. The random thermal velocities of the sample molecules must be small compared with the electron velocity. This will be true for all electron velocities and gases of interest.
2. The interval 1/f between source impulses must be long enough in comparison with T to avoid ambiguity in the inferred velocity.
3. The source must not continue to emit electrons, even weakly, after the main burst has terminated. This requirement has presented some difficulty.
4. The counting rate must be low compared with the source repetition frequency to reduce deadtime losses in counting, and long exposure times are required to insure adequate statistical accuracy; this apparent disadvantage is offset by greatly improved discrimination against background electron emission and by

multichannel TOF registration, in which the transmissions of electrons in a wide range of energy are measured simultaneously.

5. Ideally, the presence of the sample gas must not affect the emission and detection processes; in practice, these effects can be separately determined and appropriate corrections made.
6. Electrons must reach the detector only via direct paths, not involving deflections by stray fields, collisions with gas molecules or reflection from surfaces bounding the drift region. This has been a difficult requirement to satisfy.

2.3 Flight Path Geometry

The velocity v and corresponding kinetic energy eV of an electron are related to its time of flight T over a path length L by

$$v = L/T = \sqrt{2\eta V} = 5.331(5)\, V^{0.5} \text{ m sec}^{-1} \qquad (1)$$

The spectrometer is designed for transmission measurements with electrons ranging in energy from 1 eV to 0.1 eV, with the expectation of eventually extending the lower limit by at least one decade. The lowest total cross section expected is approximately $3(-21)$ m^2 (the R-K minimum in Ar).

At electron energies this low, elastic scattering is the principal contributor to the total cross section; that it is predominantly S-wave scattering is apparent from inspection of the angular distribution measurements of Ramsauer and Kollath, [14] which show nearly isotropic scattering of electrons at the lowest energies they employed, approximately 1 eV. Thus, if the solid angle subtended at the point of scattering by the electron detector is small, the great majority of all scattering events will prevent the electron from reaching the detector via a direct path; i. e., the removal cross section will be practically equivalent to the total cross section.

Experimental simplicity demands that the specimen gas fill the entire flight path from source to detector.

Under these conditions, the transmission, defined as the ratio of the number of electrons, at any given velocity range, reaching the detector

per unit time when a specimen gas fills the flight path, at pressure p and temperature θ, to the corresponding number when the flight path is evacuated, is

$$\alpha = \exp(-p\,q\,L / k\,\theta) \qquad (2)$$

In particular, a pressure p_1 exists at which the transmission is exp (-1), so that the flight distance L is then just one electron mean free path:

$$L = k\,\theta / q\,p_1 \qquad (3)$$

In order to obtain accurate values of q, it is desirable that L be long enough that the specimen gas will reduce the transmission to about this level when introduced at pressures high enough to be accurately measurable but not so high as to preclude the operation of a suitable electron detector (Sections 2.8 and 4.4). The reasonable values $p_1 = 1(-5)$ bars and $q = 1(-20)$ m^2 suggest a drift distance of 0.4 meters or more.

A second constraint is that the velocity be accurately measurable. The uncertainty in velocity determination is largely that caused by the finite time duration of the electron emission pulses (Section 3.2). Suppose this to be approximately 100 nsec. The time of flight of the fastest electron of interest must be large in comparison with it. Taking $V \leq 1$ volt, $T \geq 1$ μsec, we obtain $L \geq 0.59$ meters.

On the other hand, the difficulty of fabricating and shielding a long drift tube and the need to measure absolute specimen pressures accurately argue that L be as short as possible. A compromise value of 0.475 m was adopted.

Figure 1 presents the energy/time relationship for this flight distance. Times of flight ranging between about 0.7 μsec and 4 μsec will be involved, which can be measured with high precision if the electron emission pulses can be kept brief.

2.4 Electron Generation

Several possibilities present themselves for consideration as pulsed electron sources:

1. photoemission with pulsed illumination;

2. thermionic emission with grid control;
3. secondary emission from a surface bombarded with a gated primary electron beam;
4. emission from metal-oxide-metal films with pulsed potentials applied.

The first was chosen by elimination. The possibilities of migration of low work function material to other electrodes, of poisoning by reactive specimen gases, and of thermoelectric effects led to rejection of thermionic cathodes. The high charging currents to the film capacitance and the accompanying magnetic field disturbance eliminated the fourth possibility. The spectrum of electrons from photoemission is preferable to that typical of secondary emission, especially in assuring the absence of fast electrons from the apparatus, and it can be more readily redetermined by retardation measurements. Moreover, the fast primary beam will produce unwanted excitation and ionization of the specimen.

2.5 Electrode Materials

Constancy of contact potentials and low background electron emission demand the use of chemically stable electrode materials which have reasonably high electron work functions. Better uniformity of work function can be expected from coatings of a finely divided substance, such as colloidal graphite ("aquadag"), except for the electron emitter, which must have high quantum yield of photoemission as well as chemical stability. Gold satisfies the latter requirement.

The possibility of electrode surface contamination dictates the use of a completely bakeable system.

Using colloidal graphite, which has a work function of 4.8 volts, the thermionic emission from the drift tube walls is utterly insignificant at room temperature. The main background electron source expected is from the electron detector itself.

2.6 Magnetic Field Tolerance

Magnetic fields must be excluded. Transverse fields distort the electron trajectories, causing them to pass nearer to the drift tube surface;

axial fields confine the electrons to helical trajectories so that the axial component of velocity which is measured is not necessarily the total velocity, which determines the interaction with gas molecules in flight; either component will interfere with the removal of scattered electrons. A tolerance limit of 30 milligauss is estimated for the tranverse magnetic flux density. A stronger axial field is tolerable.

2.7 Electron Spectra

Consider a photoemitter with electron work function Φ_e surrounded by a collecting baffle of work function Φ_b (Figure 2a). These are connected through biasing batteries which supply adjustable potentials V_e to the emitter and V_b to the baffle. Let the emitter be illuminated with f equal light flashes per second. The light is not monochromatic, but has a complex spectral distribution in which λ_o is the shortest wavelength. Assume that the individual light flashes are of negligible duration. The average emitted electron current is read with an electrometer, Figure 2a.

In Figure 3, curve a) displays the so-called retarding potential (RP) curve of the time-average photoelectric current, I, from baffle to emitter. All emitted electrons reach the collector, giving the saturation current I_s, when $V_e - V_b < \Phi_b - \Phi_e$; i.e., when the applied potential difference compensates the contact e.m.f. of this electrode pair. No current flows when $V_e - V_b > \Phi_e - \Phi_b + hc/\lambda_o e$, since then the fastest emitted electron cannot surmount the potential barrier. At intermediate values of the applied potential difference, a current $I < I_s$ is collected. The derivative of curve a) is the distribution in kinetic energy of the emitted electrons, curve b) of Figure 3. The zero of the energy scale V for curve 3b) corresponds with the saturation point of curve 3a), and the area under curve 3b) is the saturation current I_s. At low energies, curve 3b) rises linearly with V; the remainder of the curve is not symmetrical, and most of the emitted electrons have energies less than half of the maximum.

By a change of scale, curve 3b) can be so normalized that its enclosed area is I_s/ef, the number of electrons emitted per flash. It then represents the probability than an electron will be emitted with energy in

a unit increment centered at the value V during any single flash, (dI/dV)/ef.

Assume now that a small aperture is opened in the baffle, admitting a small fraction β of the emitted electrons into a drift region beyond, which is finally terminated by a grid. If the saturation bias is maintained between emitter and collector, and the grid and drift tube are also properly biased as shown in Figure 2b), the transmitted electrons will travel in a field-free path and will at all times be distributed in energy according to curve 3b). Although emitted simultaneously, those electrons which were not lost enroute by collision will arrive at the grid at a distribution of times, curve 3c). We shall neglect the short additional time required to accelerate them and thereafter to effect the detection process. The probability that an electron will arrive at the grid during a time interval between T and $T + \Delta T$ will be

$$W(T)\ \Delta T = (\delta\beta/ef)\,(dI/dV)\,(dV/dT)\,\Delta T$$
$$= (\delta\beta/ef)\,(dI/dV)\,(L^2/2\eta)\,T^{-3}\,\Delta T. \qquad (4)$$

The factor T^{-3}, which arises in the relation between a unit energy interval and the corresponding TOF interval, drastically decreases the counting rate at late times. This can be shown by differentiation of Eq. (1), and seen qualitatively by inspection of curves b) and c), Figure 3. Note that the upper half of the energy spectrum, curve 3b), lies between times of flight $L/\sqrt{\eta V_{max}}$ and $L/\sqrt{2\eta V_{max}}$, differing by a factor of $\sqrt{2}$, but that its lower half is spread out over a range of T extending theoretically to infinity. Moreover, the nearly linear variation of the emission spectrum with V for low energies implies a time distribution which approaches T^{-5} at long times of flight.

The relationship of the TOF spectrum, curve 3c), to the RP curve, curve 3a), provides a very sensitive test both of the adjustment of bias and of the energy independence of electron transmission of the apparatus. Note also that the spectrum of electrons leaving the emitter can be determined by retardation measurements even when a specimen gas has been introduced for a transmission measurement, since the distance to the baffle is

small in comparison with the flight path. One can thereby determine whether changes in contact emf of the emitter with respect to the baffle are caused by the specimen gas, and if so, readjust the emitter potential to compensate them.

Equation (4) suggests a method for measuring the photoelectron spectrum directly, rather than its integral, which is measured by the conventional retarding potential technique. By eliminating differentiation of data, one should hope for greater precision in the measurement. One counts electrons reaching the detector in a fixed time interval (T, T + Δ T) as a function of the bias applied between emitter and baffle, and thus sweeps the emission spectrum across a "window" of constant energy. This has been found very difficult in practice because of the strong refraction which takes place at the baffle aperture when other than the precisely correct bias is applied to each electrode. The factor β is not in general energy-independent, and, as in any electron lens, is a function of the difference in fields on the two sides of the aperture.

The ideal potential distribution shown in Figure 2b) is of course not precisely attainable in practice. Contact potential irregularities on the drift tube walls will cause the true potential along the electron trajectory to vary slightly above or below the level line desired. These variations will be far less, however, than would be the case were the electron required to pass close to the perturbing region as in deflection apparatus. Nevertheless, they establish a minimum energy at which an electron can be transmitted, and they refract electrons of slightly higher energy. Thus, the time of flight spectrum can fall below the predicted T^{-5} distribution for very long times of flight.

2.8 Electron Detection

Three methods of single-electron detection were investigated. A particularly important consideration is that of monitoring the sensitivity of the detector, which must be exposed to the specimen gas.

Electron multipliers are readily available with demountable structures of high work function, capable of single-electron detection, and their

detection efficiency can be measured and controlled. Their background emission is of the order of 1 electron cm^{-2} min^{-1}, which is very low. [15]

Phosphor-photomultiplier combinations are more complicated and no direct relationship is known from which their detection efficiency can be inferred.

Semiconductor detectors [16] have the disadvantage of requiring at least 10 kV of acceleration potential before the electrons can penetrate to the sensitive junction layer.

The average gain of an r-stage electron multiplier with secondary emission coefficient ϵ is ϵ^r. It can be varied by adjusting the interdynode voltage. Typically, $\epsilon = 2.8$, and the overall gain is 5.1 (6). With an amplifier input capacitance of 3000 pf this will generate a 270 μV signal, well above the noise level expected for a good transistor preamplifier. The corresponding fraction of all single electron impacts which fail to generate secondary electrons is exp $(-\epsilon)$, if the secondary emission process obeys Poisson statistics, a common assumption. [17] In the example, this is approximately six percent. Thus the sensitivity and detection efficiency are not only adequate, but measurable in use by determining the distribution of avalanche multiplicities, and are controllable by adjustment of the applied voltage.

In practice it has been found that the single assumption of Poisson statistics does not explain the observed distribution of avalanche sizes. A statistical theory, which assumes that the dynodes are inhomogeneous, has been described which accounts quantitatively for these observations and allows the detection efficiency to be estimated. [18]

According to this theory, the various individual electron avalanches will have the distribution of amplitudes

$$P_r(Q, \epsilon) = \left[(\epsilon-1)^2/\epsilon^{r+2}\right] \exp\left(-Q/e\epsilon^r\right) \qquad (5)$$

It follows that the secondary emission ratio can be evaluated from the mean pulse amplitude which the charge Q produces on the amplifier input capacitance.

$$\epsilon = (\langle Q \rangle / e)^{1/r} \qquad (6)$$

The detection probability can be shown to be simply

$$\mu = 1 - 1/\epsilon = 1 - (\langle Q \rangle / e)^{-1/r} \qquad (7)$$

2.9 Counting Rates and Resolution

The need for reliable operation of an intense spark source suggests a repetition frequency of the order of 1 kilohertz. Multichannel equipment commercially available also recycles at frequencies of this order. It is designed to deal with input counting rates considerably less than the recycling rate, since the first count received after the start of a cycle disables the apparatus for the duration of that cycle. Thus, total electron counting rates must be restricted to the order of 10 sec^{-1} or less by appropriate adjustment of design variables.

Three additional factors must be included with Equation (4) if it is to relate correctly the actual counting rates to the design. The grid and accelerating field configuration may not transmit all the electrons which arrive at the grid; the electron multiplier has limited detection probability; and the amplifier system must discriminate against noise by rejecting signals below a minimum size. The factors γ, the grid transmission, μ, the detection efficiency, and δ, the discrimination factor, all less than unity, account for these considerations.

The total recorded in the n-th channel of a linear multichannel TOF analyzer operated for time τ with an instantaneous emission burst and fast detector, will therefore be

$$R_n = \frac{\alpha \beta \gamma \delta \mu \tau}{e} \left(\frac{dI}{dV}\right) \frac{L^2}{2 \eta T_1^2 (n - n_o)^3} \qquad (8)$$

where T_1 is the time-width of each registration channel, and n_o is the ordinal number of the zero TOF channel.

If the duration of the electron emission pulse or spread in detection time delays exceeds the channel width, we must write the more general expression

$$R_n = \frac{\delta \mu \tau}{ef} \left(\frac{dI}{dV} \Big|_{K/n^2} \right) K \sum_{n_i=0}^{n_{max}} \frac{\alpha \beta \gamma S(n_i)}{(n - n_i)^3} \qquad (9)$$

in which $S(n_i)$ is the value of the normalized resolution function, essentially the shape of the emission pulse given in terms of time $n_i T_1$, K is the calibration constant

$$K = L^2 / 2 \eta T_1^2 . \qquad (10)$$

and those transmission factors which may be functions of electron velocity are placed under the summation sign.

Summing Eq. (8) over all channels (or Eq. (4) over all energies and adding the transmission and detection factors) we obtain the condition

$$\Sigma R_n / \tau = \alpha \beta \gamma \delta \mu I_s / e \geq 10 \text{ sec}^{-1} . \qquad (11)$$

The baffle transmission factor β can be as high as 1(-4) without spoiling the geometry. The other factors are at most of order unity. Thus the minimum required photoelectron emission is 1.6 (-14) amperes. A greater current is desirable for improved precision of measurement and will allow more leeway in the transmission and detection factors, especially β.

With care in design, the uncertainty in flight path L can be reduced to negligible proportions, because the source and detector are both well-defined surfaces, unlike their neutron analogs. The principal uncertainty in the energy measurement, as noted, is in the TOF determination.

The spread of avalanche transit times in electron multipliers is a Gaussian of approximately 10 nsec half width. [15] Using 100 rectangular time channels, each of 40 nsec width, and a Gaussian source burst of 100-nsec half width at half maximum, we obtain what is still an essentially Gaussian resolution function dominated by the time distribution of electron emission. The resulting TOF resolution is approximately 0.25 microseconds per meter.

In Section 4.3 it is shown that the resolution function can be determined directly in use of the apparatus.

Theoretically the energy resolution

$$\frac{\Delta V}{V} = 2 \frac{\Delta T}{T} \qquad (12)$$

is inversely proportional to the time of flight. For example, with the design flight path, constant channel width and the source burst duration given above, the energy resolution is 20 percent at T = 1 μsec, 10 percent at T = 2 μsec and 5 percent at T = 4 μsec. For this to be realized in practice, exposure times must be long enough to insure adequate statistical accuracy in all channels.

Higher resolution can be realized if the resolution function is known and can be unfolded from the data (Section 5.3).

III. DESCRIPTION OF THE VELOCITY SELECTOR

3.1 Essential Components

The velocity selector comprises a vacuum system, a pulsed light source and condensing lens, photoelectron emitter and baffle, shielded drift tube, accelerating field and electron detector, together with electronic equipment for amplification, analysis, monitoring, calibration and data readout. Additional apparatus is provided for controlled introduction of sample gases at known pressure and temperature. A schematic diagram is given in Figure 4 and a photograph in Figure 5.

3.2 Pulsed Light Source

The high electron work function of the emitter calls for an ultraviolet light source. This is a spark between center conductors of two 3-meter sections of 52-ohm coaxial line, somewhat like that described by Beams.[19] The first section of line is connected to a high voltage supply through a 1-megohm series resistor; the second section is terminated by an air-cooled matching resistor. This constitutes a relaxation oscillator. The first section charges until the gap breaks down; this applies a voltage step, approximately half of the breakdown voltage, to each section of the line. The negative step applied to the first section reflects from its essentially open end, and returns to reduce the potential of its spark electrode to nearly zero. The positive step applied to the second section is absorbed in its termination. The discharge current of 100 amperes flows for about 50 nanoseconds, and then is rapidly terminated.

Figure 6 shows the spark gap cell. The electrodes are of tungsten, each constituting a smooth continuation of the center conductor of its respective coaxial line. The outer conductors of each line are continued to the wall of the spark cell by metal bellows which can be adjusted to align the gap, care being taken to preserve constant line impedance up to the gap itself. A conical hole in the cell wall with its apex located near the spark allows light to emerge through a fused quartz window.

The cell is filled with hydrogen at a gauge pressure of 1 5 bars with 0.030-inch gap spacing. More light is emitted at higher pressures

and voltage, but the waveform becomes unsatisfactory and electrode wear becomes excessive.

The repetition frequency, approximately the product of the reciprocal of the time-constant of the recharging circuit by the ratio of applied to breakdown voltages, is controlled by varying the applied high voltage. The normal repetition rate is 10^3 sparks/second at 5500 volts.

Adjustments are provided to position an image of the spark in UV light at the proper point on the emitter which maximizes the electron counting rate.

Many other possible light sources have been considered but found inadequate or impractical. Q-spoiled lasers are not yet available for far ultraviolet and have too low repetition frequency. Kerr cells or mechanical choppers are inconvenient for ultraviolet and require too high source brilliance to be practical. Considerable effort was expended on an alternative source, also a spark gap, but in air, short circuiting a small plane capacitor with mica dielectric by means of electrodes very close to the capacitor elements, Zinc electrodes were tried because of the intense ultraviolet resonance line at 2139 Å, but it was found that imprisonment of resonance radiation in the Zn vapor unduly extended the duration of the light emission; when tungsten electrodes were substituted for zinc, persistent components were still observed in the air spark. The least after-luminescence was found with tungsten electrodes in hydrogen. The mica capacitor source then had excellent pulse form, but at normal repetition rates, had unduly short lifetime in hydrogen. Its replacement by an equivalent capacitance led naturally to the present design.

3.3 Vacuum System and Specimen Gas Supply

A 40-liter/second ion pump and sorption-type rough pump are mounted at the lower end of a vertical manifold of 4-inch stainless steel tubing with stainless steel flanges, assembled with heliarc welds and copper gaskets. This is wrapped with electrical heating tape for bakeouts and covered with 2-inch thermal insulation (Figures 6 and 7). The manifold is 2 meters in length, thus isolating the drift region at the upper end from the magnetic field of the ion pump.

For transmission experiments the system is provided with electrically controlled selective leaks for He, O_2, and H_2, together with an adjustable orifice for use with other gases.

Relation of the measured electron attenuation to the total cross section (Equation 2) requires that the absolute molecular concentration of the specimen in the drift region be known. For the noble gases, the pressure p_1, (Equation 3) at ambient temperature is between 0.2 and 10 μbars. The only absolute instrument available in this pressure regime is a McLeod gauge. However, to prevent contamination of the electrode surfaces by mercury, it is necessary to isolate the main system from the McLeod gauge. A cryogenic trap is not suitable, because of the pumping action of the condensing mercury. [20] Ionization gauges, though available for this pressure regime, are found to produce an inadmissible background count, proportional to the sample pressure. The best solution found to this problem is a diaphragm capacitance manometer with an ionically pumped reference system. This was calibrated at higher pressure with a McLeod gauge and trap on the reference side of the diaphragm, and found to be linear, when compared with an ionization gauge at lower pressure.

3.4 Magnetic Shielding

The irregularity and variability of ambient magnetic fields in the laboratory precludes their compensation by any convenient arrangement of coils or permanent magnets. Moreover, the stainless steel envelope is made locally magnetic by welds. Shielding of the drift tube by concentric layers of high permeability alloy is the only practical method of reducing the magnetic flux density below tolerable levels (Section 2.6).

Two concentric cylinders of annealed molybdenum permalloy are mounted inside the vacuum enclosure coaxial with and extending beyond the drift tube and are electrically grounded to the envelope. The axial component of magnetic flux, measured with a Hall-effect gaussmeter, is reduced from the ambient 0.4 gauss to under 10 milligauss in the drift region except near the detector end of the drift tube; there, an auxiliary degaussing coil compensates for most of the ambient field and so extends the effective length of the longer, outer shield cylinder.

Additional cylinders of magnetic shielding enclose the electron multiplier structure and extend outward from the two openings in the main magnetic shield which admit the emitter-baffle assembly and light from the spark source.

3.5 Electron Emitter

The emitter was adapted from a commercial indirectly-heated thermionic cathode assembly by substituting a thimble of gold-plated molybdenum with a hemispherical end for the thoriated-tungsten sleeve of the cathode. The internal heater is useful for outgassing the emitter. The electron emission originates in an UV image of the spark on the upper quadrant of the hemisphere positioned (Section 3.2) by adjustment of the spark cell (Figure 6) at the intersection of the common axis of the drift tube, magnetic shield and vacuum enclosure with the line through the optical centers of the lens and spark. This adjustment is made by plotting electron counting rates against readings of verniers on the spark cell mounting.

3.6 Lens-Window

A 2.5-inch diameter lens, ground and polished from a disc of high quality fused quartz to a 10-cm focal length (at λ = 2200Å), doubles as a vacuum-tight window and as a condenser to image the spark source on the emitter. A camera shutter and iris diaphragm can be closed for background measurements and adjusted to reduce the level of emitter illumination to yield about 1000 photoelectrons per spark (Figure 6). As this requires a relative aperture f 44, the chromatic aberration, though observable, is not serious.

3.7 Baffle

Early tests with a solid drift tube showed that it is necessary to intercept and remove electrons emitted in directions other than toward the detector. The baffle, which performs this function, is an aquadag-coated titanium cylinder coaxial with the cylindrical body of the emitter, as diagrammed in Figure 4. A small aperture is drilled adjacent to the illuminated spot on the emitter hemisphere. Only 4(-5) of the emitted

electrons normally will pass through this aperture into the drift tube. The remainder are collected on the baffle and monitored with an electrometer.

The long cylinder form of the baffle effectively isolates the emitter from electric fields penetrating from the open end, but allows entry of light directed along its axis to excite photoemission.

3.8 Drift Tube

The drift tube comprises two concentric cylindrical arrays of parallel aquadag-coated 0.01-inch molybdenum wires inside a helical grid of heavy molybdenum, also aquadag-coated. The open structure allows escape of electrons scattered out of the beam defined by the baffle aperture; a bias is applied to insure that these will be collected by the vacuum envelope or magnetic shield. A shielding apron encloses the region adjacent to the baffle. It was necessary to fabricate this element in the laboratory since grid structures of acceptable materials and mesh size were not commercially available. An extension of the principle of the slat grid to radial geometry (see Section 3.9) suggests an improved design for future work: a radial array of long plane strips extending parallel to and coaxial with the electron drift path.

3.9 Grid

Beyond the drift tube, an electron enters a short region of strong electric field which imparts energy sufficient for its detection (Figures 2 and 4). One cannot employ a conventional wire grid to separate the two regions, since the transverse components of electric field in the neighborhood of the grid wires scatter most of the incident slow electrons. A succession of grids is little better in this respect. The solution to this problem, termed a "slat-grid", is an array of plane conducting strips, spaced apart about one-fifth their common width, mounted at the upper end of the drift tube with the slats aligned in the direction of the system axis (Figure 8).

The electric potential in the space of thickness s between any pair of adjacent strips has the approximate form $\left(\sin \frac{\pi x}{2s}\right) \left(\sinh \frac{\pi y}{2s}\right)$, if the

distance x is measured from the median plane normal to the strips, and y, from the incident, field-free edge in the median plane parallel to the direction of incidence. A field of this form can be shown to have a focusing property; i.e., electrons incident from the field-free side in directions inclined only slightly to the drift axis will oscillate with diminishing amplitudes about the median planes, while accelerating steadily, emerging near the median plane so as to avoid fringing fields at the high-field side, and directed toward the detector (Figure 8).

A cylindrical shield enclosing the acceleration space between the grid and the detector is biased negatively, so as to focus the electrons emerging from the grid onto the more sensitive central area of the detector, and to prevent electrons scattered from the drift tube from reaching the detector via indirect paths.

3.10 Detector

The detector (see Figure 7) is a demountable 15-stage electron multiplier, EMI type 9603B. In normal operation the first dynode is 200 volts above ground potential and the interstage voltage is also 200 volts. The anode is at 3000 volts above ground potential, and must be isolated from the pre-amplifier by blocking capacitors. The gain of this electron multiplier (see Section 4.2) is about 10^7 at normal operating potential.

3.11 Electronic System

A block diagram of the electronic system is included in Figure 4. Four interconnection systems are distinguished:

a) Direct biasing potentials to emitter, drift, baffle, grid, and detector shield-lens, shown as short-dash lines in Figure 4. Five decade-potentiometers with a storage battery adjust these bias potentials. The drift tube is normally biased negatively 5 volts with respect to the grounded vacuum envelope; the bias supplies to the remaining electrodes are adjusted, ordinarily so as to compensate contact emf's or for certain special tests (Section 2.8), to impart a known energy increment to the electrons. A dynamic-capacitor electrometer in series with the emitter monitors the total emission.

b) Zero-time signals, shown by heavy-dashed lines. The voltage pulse at the spark gap load resistor, attenuated, is used to initiate time-height conversion, to open registration gates, to actuate a counting rate meter and a scaler for exposure monitoring, and to trigger a monitoring oscilloscope (not shown).

c) Electron count signals, shown as dotted lines. Amplified counts from the electron multiplier are analyzed directly when received with respect to pulse amplitude by the pulse height analyzer (PHA) using channels 201-300. An anti-walk level discriminator passes counts sufficiently above noise level to the "stop" input of the time-height conversion circuit and to the electron scaler. In the time-height converter, a constant current charges a low-leakage precision capacitor during the interval between zero-time and stop-signals. The capacitor is discharged, producing a pulse of amplitude proportional to the stored charge and, hence, to the time interval between zero-time and stop pulses, into the 1-100 channel input of the PHA at readout time. The latter is delayed 120 μsec after receipt of the zero-time signal, in order that the PHA may first complete its task of amplitude registration before registering the time spectrum.

d) Gating signals, shown as single-dashed lines. These are applied to coincidence terminals of the PHA in order to restrict its registration period for detector pulse height analysis to the first 3.5 μsec after each spark, and for time analysis to a corresponding interval delayed by 120 μsec after receipt of the zero-time signal.

The total electron count above discrimination level, separately recorded by a scaler, is useful not only for monitoring, but also for low-resolution experiments and for adjustments in which the velocity distribution of the electrons is of secondary importance.

Transistorized circuits are used throughout. The preamplifier uses two 2N-2049 low-noise high-gain NPN silicon planar transistors in

a charge-sensitive feedback circuit with an effective input capacitance of 2.80 nanofarads. The main amplifier uses 2N914 NPN fast-switching transistors in three feedback stages with stepped gain control. The overall voltage gain is 1.6(3).

The PHA is a commercial 400-channel pulse height analyzer. An automatic routing feature registers the pulse amplitude distribution and the time spectrum of electron counts in separate memory groups of 100 channels, each in conjunction with its appropriate time gate, as described above.

Calibration equipment consists of a pulse generator, digital time delay circuit and a stepped attenuation network.

Figure 5 shows the complete array of racks of auxiliary equipment. Readouts are by typewriter, curve plotter, and punched paper tape.

IV. PERFORMANCE

4.1 Calibration

In normal operation, the PHA operation is checked daily with the use of calibration signals. The average width of the amplitude channels corresponds to a signal of 3.4(-6) volts, or 5.9(4) electrons at the detector output. The time channels are 25 nanoseconds wide. The overall linearity is excellent (Figure 9); pulses with equal time delay, but differing in amplitude by no more than 50 channels, will be time-registered within the same channel.

4.2 Amplitude Distribution of Electron Counts

Figure 10 shows amplitude distributions of electron counts taken under the following conditions: a) shutter closed; b) shutter open, but drift tube biased to cut off electrons from the baffle aperture; c) shutter open, drift tube biased for full electron transmission. The counts in curve 10a) are from circuit noise and dark current. The electron counts in curves 10b) and 10c) are distributed in amplitude exponentially (Section 2.8), and their mean pulse height is ample for efficient discrimination against noise. The possibility that even a small number of noise counts will be registered in late time channels, which contain few electron counts, dictates use of a high discrimination level, despite the reduced counting rate. Thus, the discrimination level, indicated in Figure 10, is 250 μV, more than the 205-μV mean pulse height of the counts in Figure 10a).

4.3 Time Distribution of Electron Counts

When the drift tube is biased negatively with respect to the emitter and baffle, electron counts are still observed. Their amplitude distribution, Figure 10b), and their time distribution, Figure 11a), demonstrate that they originate principally at the grid, being excited there by light reflected from the emitter. Additional experiments confirm this explanation. The time spread of these 'prompt' counts is determined by the waveformof the light burst and the statistical spread in times for collection and detection. The maximum of the prompt group is the effective zero time of the time analyzer system.

When saturation bias is applied to the emitter-drift system and the drift tube is also correctly biased, the time distribution is that of Figure 11b). In addition to the prompt group, a second group of electron counts now appears. These are transmitted electrons generated at the emitter. They have a minimum transit time corresponding to the fastest photoelectron emitted, and a maximum counting rate for TOF near 0.9 μsec. The counting rate falls rapidly with increasing TOF, decreasing by a factor of 10,000 in the TOF interval between 1.5 and 3.0 μsec.

Attempts to increase the low counting rates in late channels by deceleration of the more abundant photoelectrons near the maximum of Figure 3b) have not been successful, because of the strong lens action at the baffle aperture.

4.4 Effects of Specimen Gases

Figure 12 compares time spectra in two one-hour runs, identical except for the admission of helium. Note that the prompt component is unaffected but that the transmitted electrons are attenuated. Their attenuation at any channel number is exponential with sample pressure; this confirms the single nature of the scattering and disposes of the possibility that scattered electrons may arrive at the detector at later times. The distribution of detector pulse heights is unaffected by helium.

Figure 13 is a comparison of time spectra with and without argon. The transmitted electrons show the Ramsauer-Townsend effect clearly: the early transmitted electrons are strongly attenuated by the sample (pressure 8 μbars), but not those in later channels. Note, however, that the prompt peaks are not identical, despite the equality of exposure conditions; the presence of Ar broadens the prompt peak and shifts its maximum to later times. There is a greater background at very late channels in the Ar run, and the pulse height spectrum changes, becoming non-exponential after a long exposure.

Oscilloscopic observation of the detector pulses during and after an Ar run reveals that they are no longer necessarily single avalanches. Trains of several pulses, diminishing in amplitude, are often observed,

more frequently after a long exposure in Ar. The separation of these pulses, approximately 0.3 μsec., is in good agreement with the interdynode transit time of Ar^+. Normal detector operation can be restored by a bake-out and reactivation in oxygen.

These facts suggest that argon is cleaned up by the electron multiplier. At the relatively high pressures required to explore the Ramsauer minimum, electrons, which have traversed the entire length of the drift tube while at low energies, can scatter and ionize appreciably in relatively short distances when they are accelerated to the higher energies required for their detection. Because of scattering, a slightly longer time is required, on the average, for each electron to traverse the distance from the grid to the first dynode of the electron multiplier, thereby delaying the prompt peak. The probability of ionization in the 3 mm spacing between dynodes, at the pressure given in Figure 3, is approximately 0.06. Thus, most electron avalanches will create Ar^+, and it will be collected by the interdynode field. Subsequent avalanches can release it, and it will slowly migrate to earlier dynodes. Each Ar^+ impact will create a new, slightly delayed avalanche, hence the trains of pulses which are observed. The case of Ar is exceptional, however, as no other gas has so high a ratio of ionization cross section at 100 volts to total cross section at 0.2 volt.

The spectrometer has been operated for short periods with all the stable noble gases, with N_2, O_2 and H_2. No other unusual effects have been noted.

4.5 Transmission Measurement Procedure

An electron transmission experiment begins with a thoroughly baked system, with the source alignment, analyzer calibration and bias settings checked. The specimen gas is admitted, then pumped out. A retarding potential curve is measured. Open-beam time and amplitude distributions are then accumulated, with the ion pump and ion gauge shut off to keep background at a minimum. The spark frequency, average total emission, exposure duration, total cycles and electrons counted are recorded, and the stored analyzer information is tranferred into the unused half of its

memory. The gas specimen is then admitted into the spectrometer to the required pressure, read with the capacitance manometer. After waiting for thermal stabilization, a new retarding potential curve and a second set of spectra are measured, preferably with a longer exposure period, and the same quantities are recorded. The two runs are compared by visual inspection of the analyzer display, and, if satisfactory, are read out by curve plotter, by typewriter and by punched tape. The latter is then sent for computer processing (See Section 5.1) and the analyzer memory cleared, so that additional runs may be accumulated.

A typical run lasts for several hours. Electrode wear eventually requires realignment of the spark gap; so far this has limited the maximum duration of a run to four hours, although it is hoped that improvements under consideration will enable accumulation for several days.

Figure 14 shows total cross sections measured for He and Ar. The data plotted are averages from ten individual determinations, treated as described in Section 5.1. The high end of the energy scale is distorted because no resolution correction has been applied to the data (section 5.2).

V. DATA PROCESSING

5.1 Data Reduction Program

The large volume of data stored in the analyzer (memory capacity 400 channels) must be processed electronically. A program has been written, but it does not include all the features desired (Section 5.2).

The present program for the GE 625 computer accepts calibrations, monitoring and counter data collected in pairs of runs as inputs and calculates the detector sensitivity, the electron spectrum for each run, and a scattering cross section from the pair of runs.

Raw amplitude and TOF data are first corrected for deadtime losses. That portion of the corrected amplitude distribution which is above the discrimination level is fitted to a decreasing exponential function of signal voltage, from which the detector gain, corresponding detector efficiency and the fraction of all true counts above discrimination level are calculated.

The deadtime-corrected TOF spectrum is next separated into two distinct components. The peak of the prompt component is identified as the zero-time-of-flight channel and its integral obtained as a monitor of exposure. Its half-width is used to estimate the time resolution. The channel-number vs. energy relation is evaluated from the time analyzer calibration (which need not be perfectly linear) and the zero time-of-flight channel number. Differential and integral electron energy spectra are then determined from the recorded channel counts.

To compute a cross section, normalized counts in corresponding energy channels of the two runs are compared. The computer totals the deadtime-corrected counts in several adjacent groups of data channels where necessary to exceed a specified statistical accuracy requirement. This is essential for the very late low energy channels. The outputs are the effective energy and energy width of the channel group, the electron transmission, the corresponding total cross section, and its statistical error.

5.2 Resolution Correction

The energy and cross section values so computed are correct for late channels, but are systematically displaced for the very early channels

because of the finite time resolution. Thus, the energy values in Figure 14 are not correct near one volt.

Before calculating either electron spectra or cross sections, it is desirable to unfold the resolution function from the recorded distribution of counts among the various channels, to obtain the true TOF distributions. Since the resolution functio ~ and the normalization factor are contained in the prompt group, it seems advantageous to use the latter directly as a basis for unfolding the data. The obvious procedure to this end is to solve the finite system of algebraic equations which corresponds to Equation 9, of the form

$$\sum_{i=1}^{100} S_{ij} f_i = g_j, \quad j = 1.....100 . \qquad (13)$$

Here g_j are the deadtime-corrected TOF distribution data recorded in 100 channels, f_i are the unknown resolution-corrected data which would correspond to the actual TOF distribution, and the matrix $S_{ij} = S(n_j \rightarrow n_i)$ is the appropriately weighted resolution function (see Equation 9).

This system can be solved, in principle, by either matrix inversion or iteration, and it would seem particularly simple to use the prompt group as the basis for the S-matrix. However, statistical fluctuations preclude direct application of this procedure with the actual counter data, yielding an inverse matrix which is useless, or failing to converge on iteration. Before the resolution correction can be applied, the data must be smoothed to a well-behaved functional form. This function is presumably known a priori for the open beam case, but not for the transmitted spectrum with a sample present; in fact, the objective of the experiment is to determine it! In neutron spectroscopy, the functional forms are known; moreover, open-beam counting rates do not vary widely over a wide range of TOF so that all of the data have comparable statistical accuracy.

VI. ACKNOWLEDGMENTS

This project has benefited from the experience, assistance and encouragement of others than the authors. The encouragement of Mr. T. W. Dietze and of Professor Emeritus L. B. Loeb of the University of California consultant, are especially acknowledged. The authors are indebted for technical assistance to E. A. Taft, P. D. Johnson, L. A. Harris, H. Coghill, G. Jernakoff, D. Schaefer, R. Girard and T. W. Hickmott of the General Electric Research and Development Center, to S. Mintz of the Technical Information Processing Operation and to R. Hummer of the Schenectady Tube Operation. Prof. G. P. Calame of Rensselaer Polytechnic Institute has been helpful in the development of the computer program.

DEFINITION AND SYMBOLS

v	electron velocity (meters/second)
L	drift distance (meters)
T	time of flight over drift distance (seconds)
η	electron charge÷ electron mass (coulombs/kilogram)
V	electron energy ÷ electron charge (volts)
α	ratio of electron arrival rate at grid with specimen to that with no specimen in the drift path, all other conditions being equal
p	pressure of specimen gas (joule/m^3)
q	total cross section of specimen molecule (m^2)
E	Boltzmann constant (joule/^oK)
θ	specimen pressure at which L = electron mean free path (joule/m^3)
$w(T)$	probability per unit time that an electron will reach the grid (sec^{-1})
β	transmission efficiency of baffle aperture
γ	transmission efficiency of grid
f	recycling frequency of the apparatus (sec^{-1})
I	photoelectric current from baffle to emitter (amperes)
I_s	saturation value of I (amperes)
$P_r(Q,\epsilon)$	probability of an output electron avalanche containing Q/e electrons from single electron impact on the first dynode of an r-stage electron multiplier of mean secondary emission coefficient ϵ
Q	charge in a single detector output avalanche (coulombs)
$<Q>$	average value of Q
ϵ	mean secondary emission coefficient of detector
r	number of dynode stages of detector
μ	probability that single electron impact on the detector will produce an avalanche at the output
R_n	count registered in channel n of the time analyzer
n	ordinal number of multichannel PHA
δ	fraction of all electrons detected which produce avalanches above discrimination level
τ	accumulation time of experiment (seconds)
T_1	time interval corresponding to one analyzer channel (seconds)

n_o ordinal number of time analyzer channel which corresponds to the mean electron emission time

K time analyzer calibration constant, $L^2/2\eta T_1^2$, (volts)

S_{ij} resolution function for time analysis

REFERENCES

1. Kieffer, L. J., "A Bibliography of Low-Energy Electron Collision Cross Section Data," JILA Information Center Report No. 2, University of Colorado, April 1, 1966.
2. S. C. Brown, Basic Data of Plasma Physics, John Wiley & Sons, Inc., New York, Chapter 1, (1959).
3. L. B. Loeb, Basic Processes of Gaseous Electronics, University of California Press, Berkeley, p. 216, 1st Edit. (1955
4. Houston, J. M., "Cross Section Values to Use in Analyzing the Cesium Thermionic Converter," Proceedings of the IEEE Thermionic Conversion Specialist Conference, Cleveland, Ohio, and General Electric Report 65-RL-3859E, January 1965.
5. Massey, H. S. W. and Burhop, E. H. S., Electronic and Ionic Impact Phenomena, Oxford University Press, London (1956).
6. R. B. Brode, "The Quantitative Study of the Collisions of Electrons with Atoms," Rev. Mod. Phys. 5, 257 (1933).
7. Ref. 5, Section I.5.
8. J. A. Simpson, "High Resolution Low Energy Electron Spectrometer," Rev. Sci. Insts. 35, 1698 (1964).
9. C. Ramsauer and R. Kollath, "Effective Cross Sections of Rare Gas Molecules for Electrons Under One Volt," Ann. der Physik 395, 536 (1929).
10. D. E. Golden and H. W. Bandel, "Absolute Total Electron-Atom Scattering Cross Sections for Low Electron Energies," Phys. Rev. 138, A14, (1965).
11. D. E. Golden and H. W. Bandel, "Absolute Total Electron Scattering Cross Sections in H_2 and D_2 for Low Electron Energies," Phys. Rev. 146, 40 (1966).
12. T. F. O'Malley, "Extrapolation of Electron-Rare Gas Atom Cross Sections to Zero Energy," Phys. Rev. 130, 1020 (1963).
13. G. C. Baldwin and S. J. Friedman, "Electron Spectrometer for Measurement of Low Energy Collision Probability," Bull. Amer. Phys. Soc. 9, 53 (1964).

14. C. Ramsauer and R. Kollath, "The Angular Distribution of Scattering of Slow Electrons by Gas Molecules," Ann. der Physik, 12, 837 (1932).

15. J. A. Sharpe, Nuclear Radiation Detectors, Methuen and Co., Ltd., London, Chapter V, (1955).

16. S. S. Friedland and R. P. Ziemba in Methods of Experimental Physics, ed. by L. Marton, Academic Press, New York, Vol. 5, Chapter 1.8 (1961)

17. F. J. Lombard and F. Martin, "Statistics of Electron Multiplication," Rev. Sci Insts, 32, 200 (1961).

18. G. C. Baldwin and S. I. Friedman, "Statistics of Single-Electron Multiplication," Rev. Sci. Insts, 36, 16 (1965).

19. J. W. Beams, "Spark Light Source of Short Duration," Jour. Opt. Soc. Amer. 37, 868 (1947).

20. F. DeVries and P. K. Pol, "Theoretical and Experimental Determination of an Error in the Pressure Indication of a McLeod Manometer," Vacuum 15, 135 (1965).

Figures

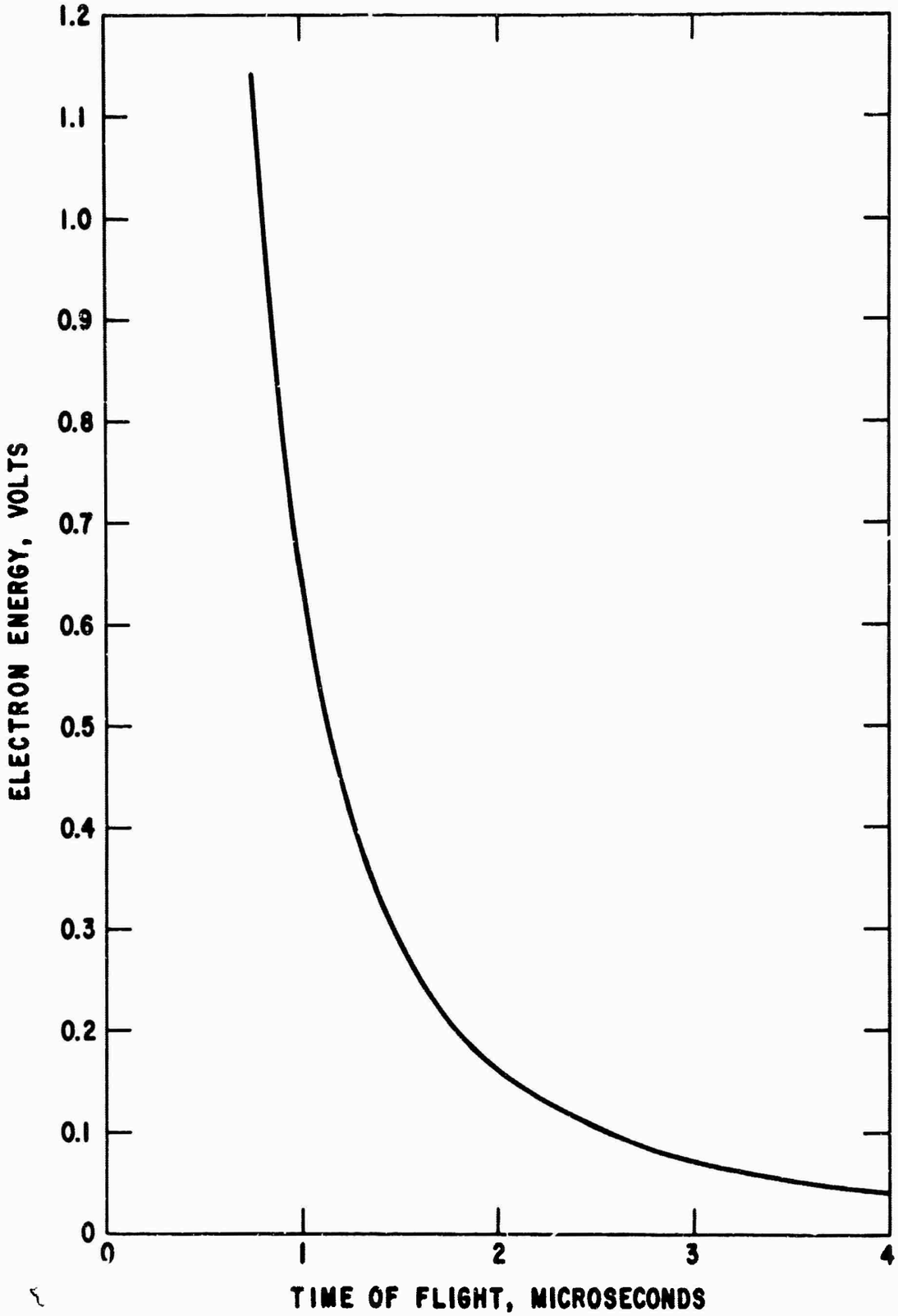

Figure 1. Kinetic energy of an electron vs time to traverse a 0.475-meter flight path.

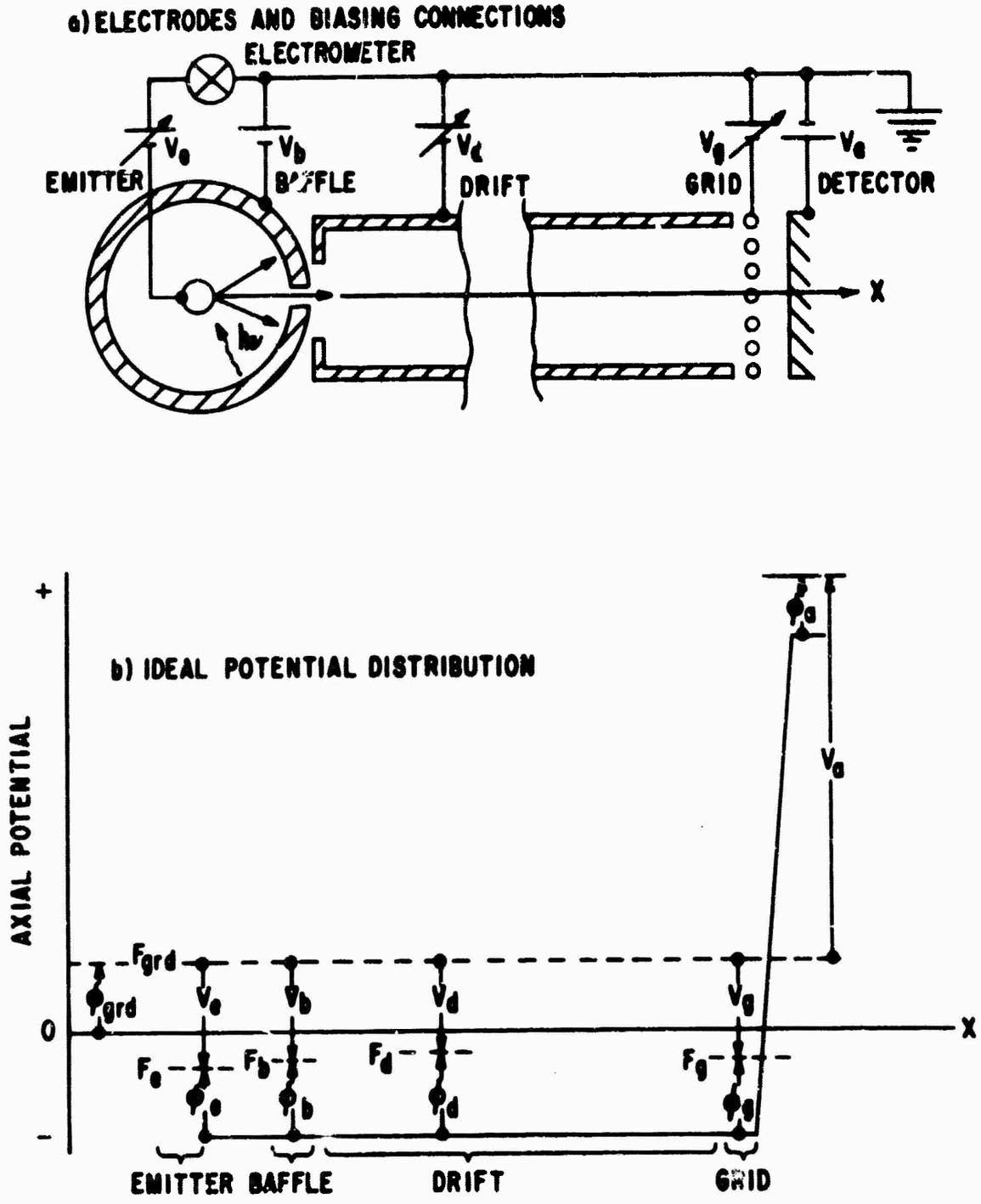

Figure 2. Essential electrodes and biasing requirements for TOF electron velocity selection. The electrode arrangement, diagrammed in (a), includes a baffled photoelectric source, drift tube, grid and detector. Each must be appropriately biased, as shown in (b), to establish uniform electric potential along the electron path. In (b), the dashed lines represent the respective Fermi level of each electrode.

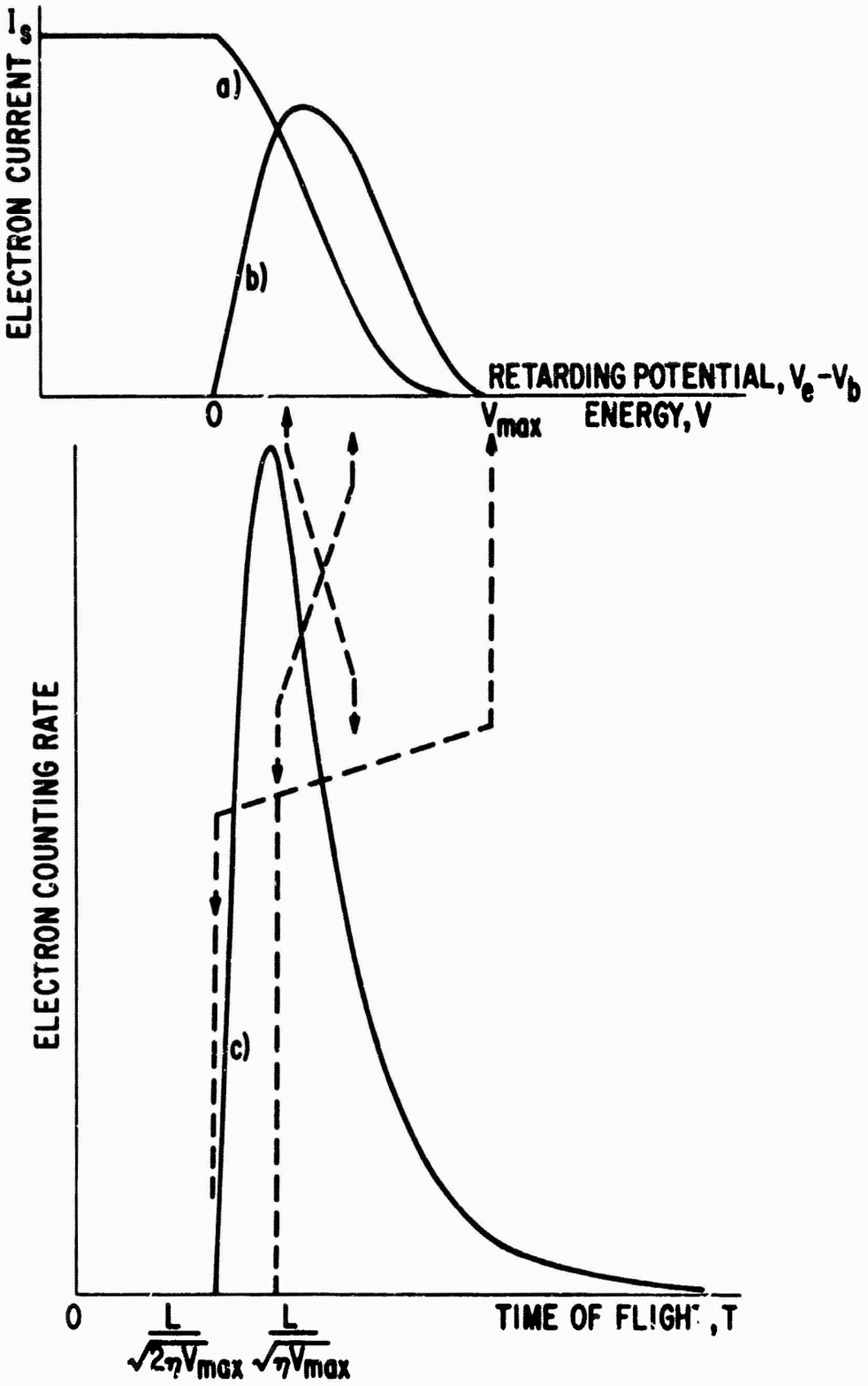

Figure 3. Relationships of (a) integral and (b) differential energy spectrum of photoelectrons to the distribution of times of flight, (c).

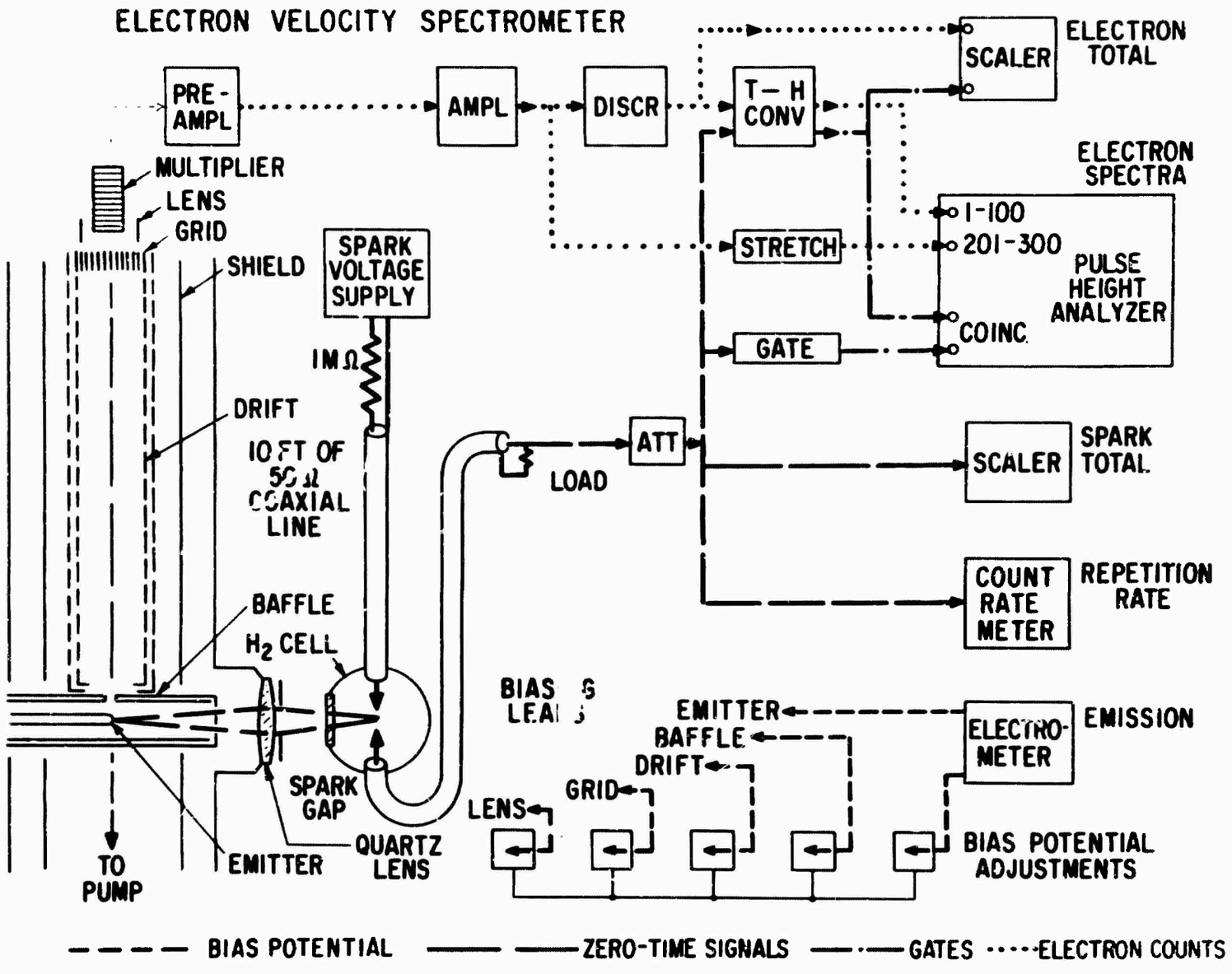

Figure 4. Schematic diagram of the electron TOF spectrometer.

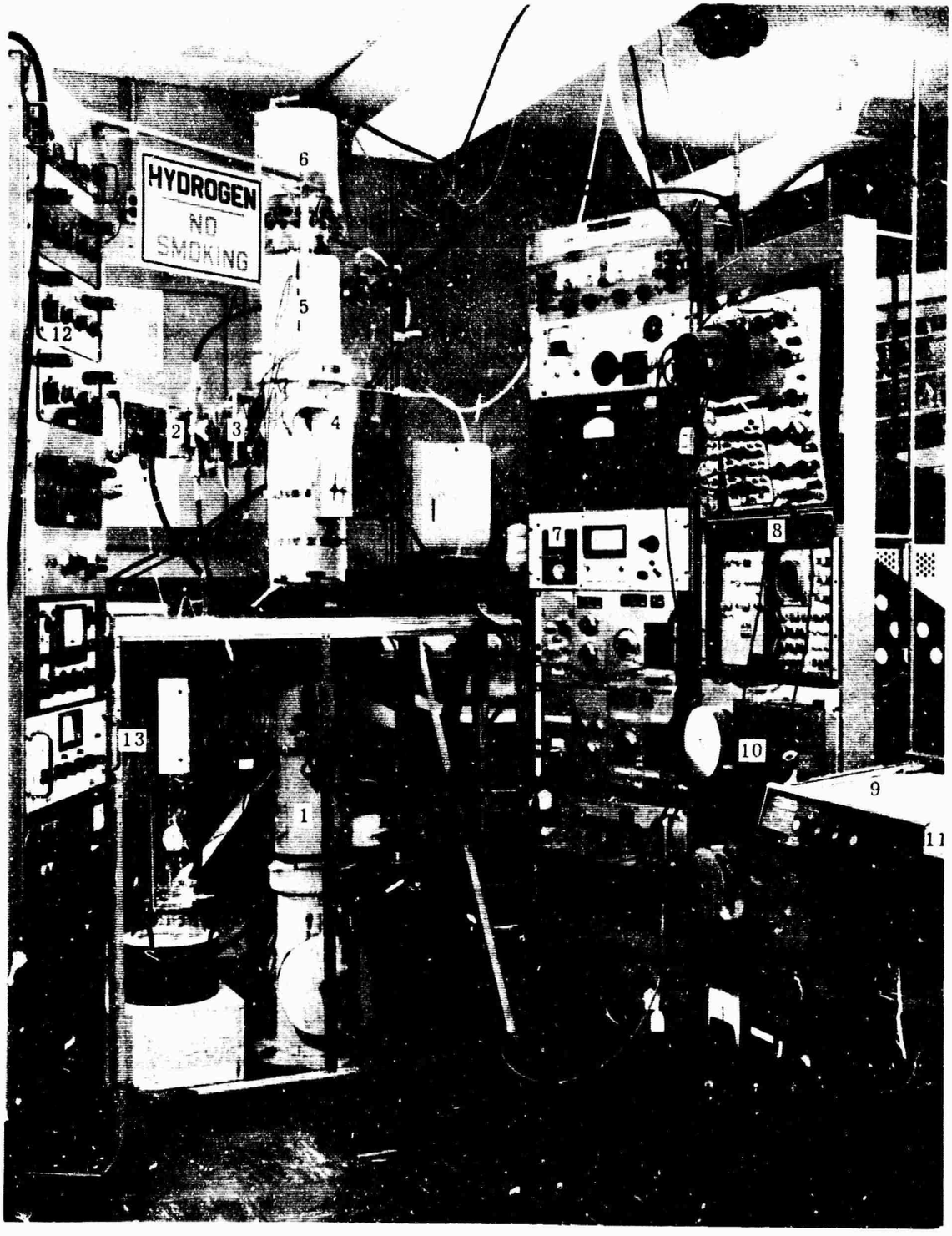

Figure 5. Photograph of complete electron TOF spectrometer: (1) vacuum enclosure; (2) pulsed light source; (3) lens-window; (4) emitter-baffle-electrometer; (5) drift region enclosure; (6) detector-preamplifier enclosure; (7) monitoring and calibration apparatus; (8) multichannel analyzer and readout units; (9) plotter; (10) punched tape readout; (11) typewriter readout; (12) biasing potentiometers; (13) specimen pressure manometers.

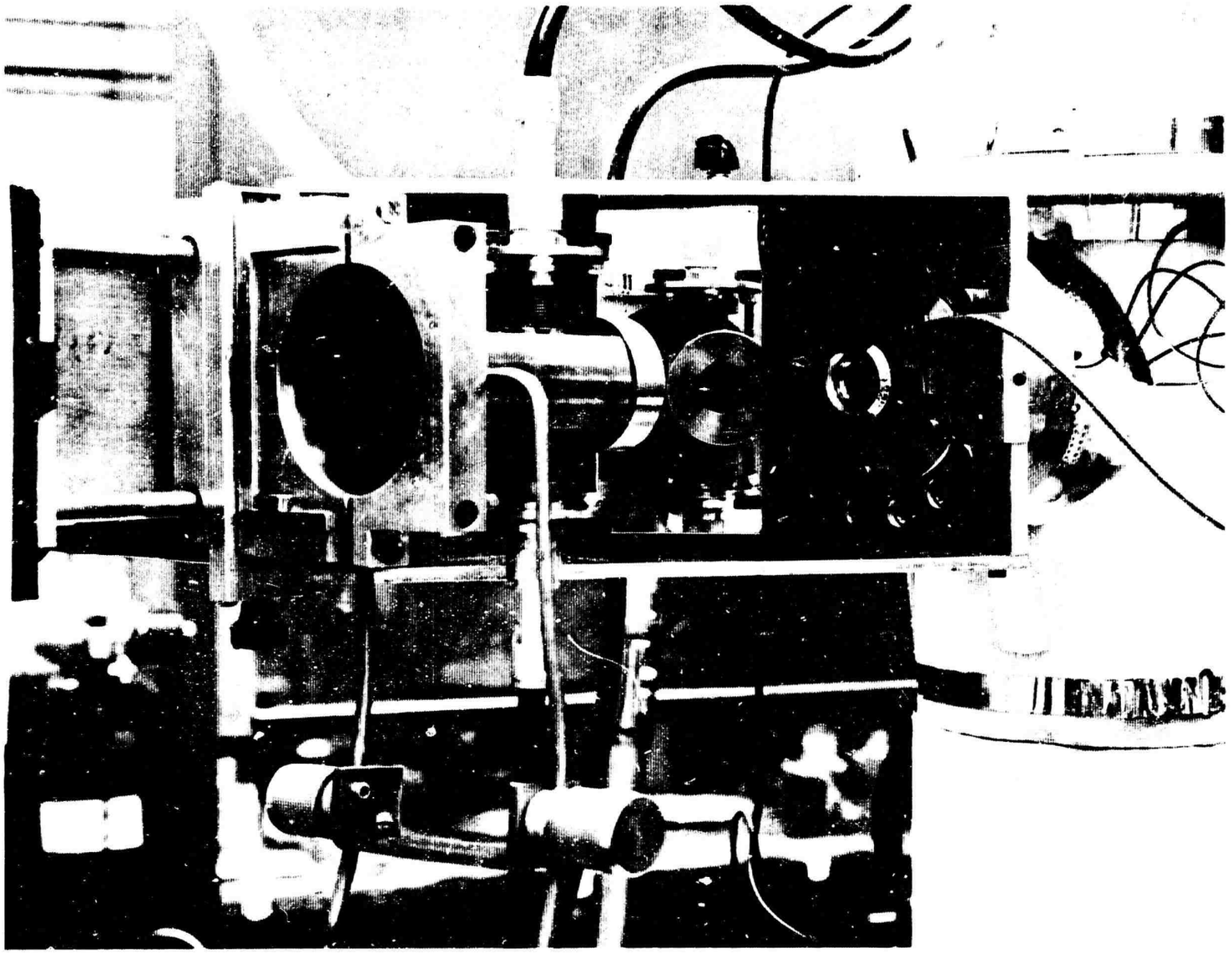

Figure 6. Pulsed light source and lens-window. The spark can be seen in the reflecting mirror.

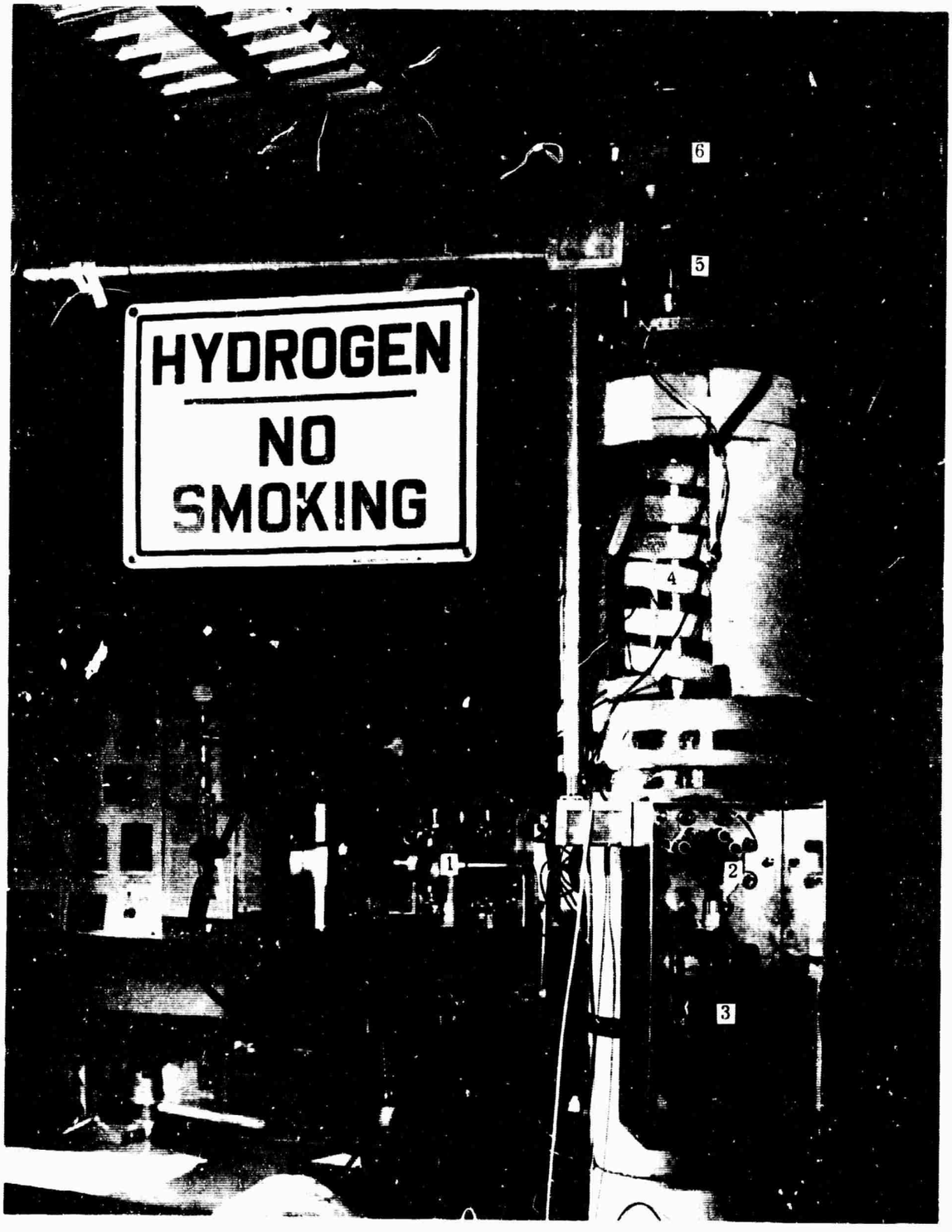

Figure 7. Closeup of the spectrometer with housings and insulation partially removed, showing: (1) light source; (2) emitter-baffle flange; (3) electrometer preamplifier; (4) heating tape; (5) detector; (6) preamplifier.

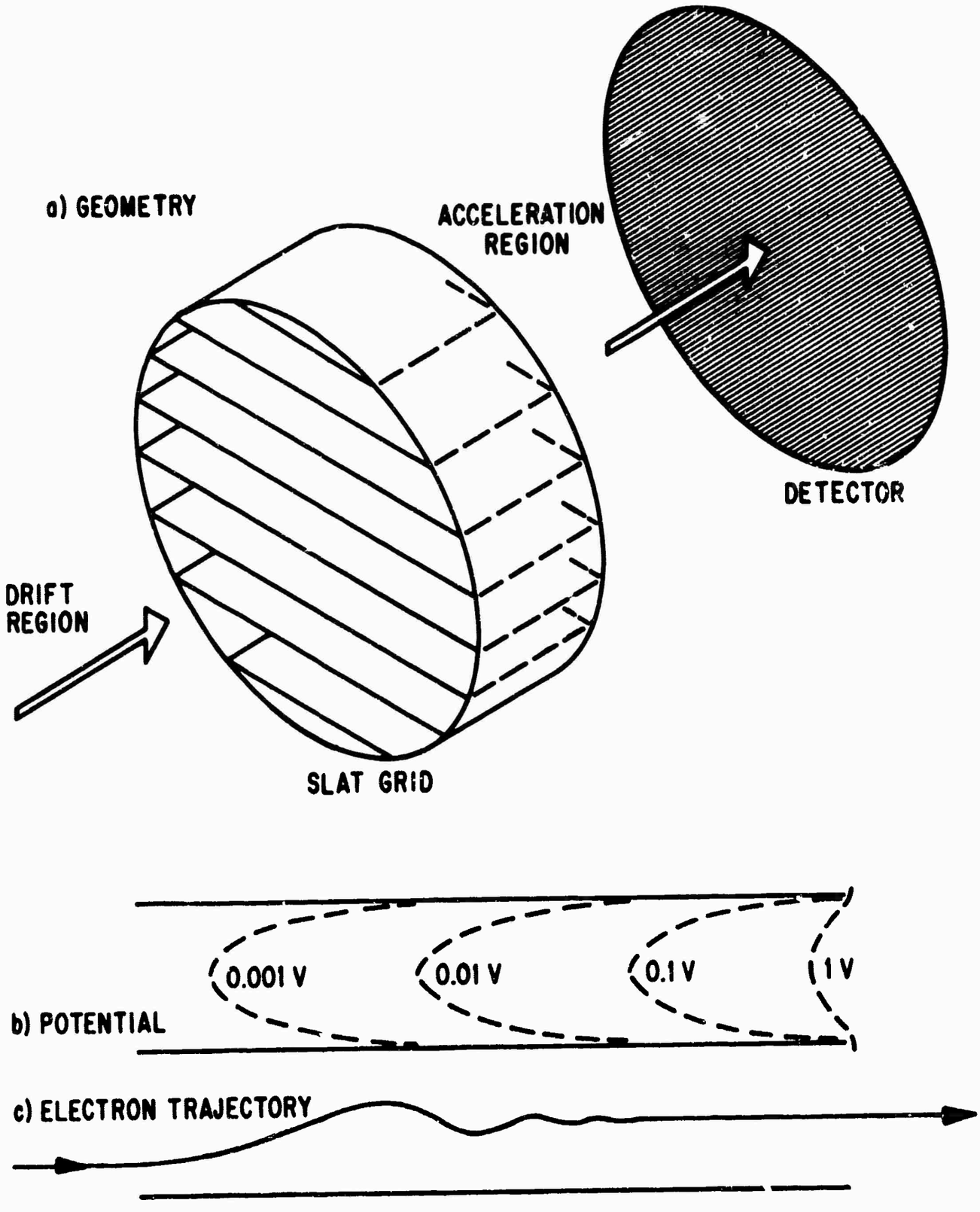

Figure 8. The slat grid: (a) geometry; (b) electric potential between adjacent slats; (c) trajectory of an electron passing through the grid.

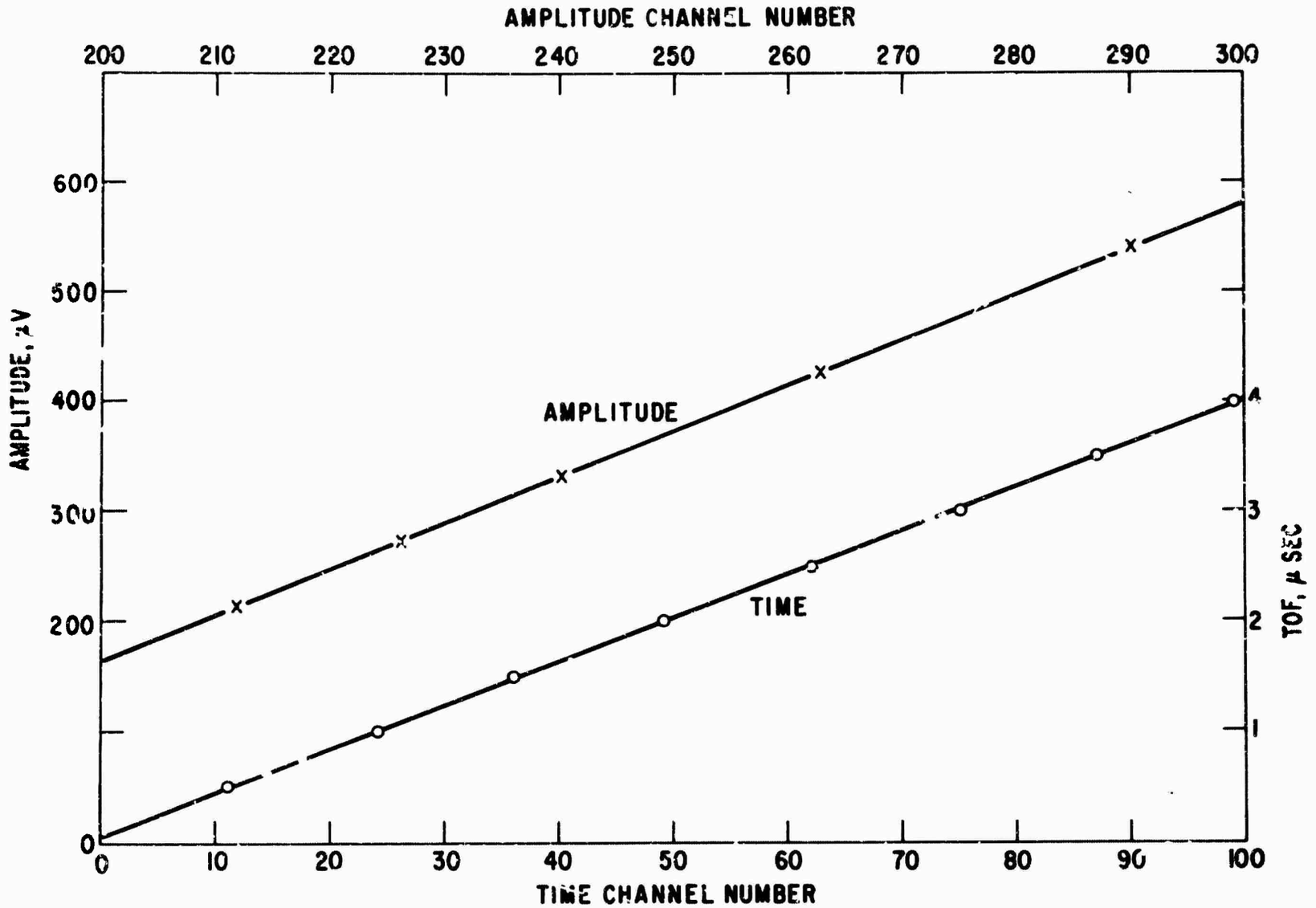

Figure 9. Calibration of the multichannel amplitude and time analyzer.

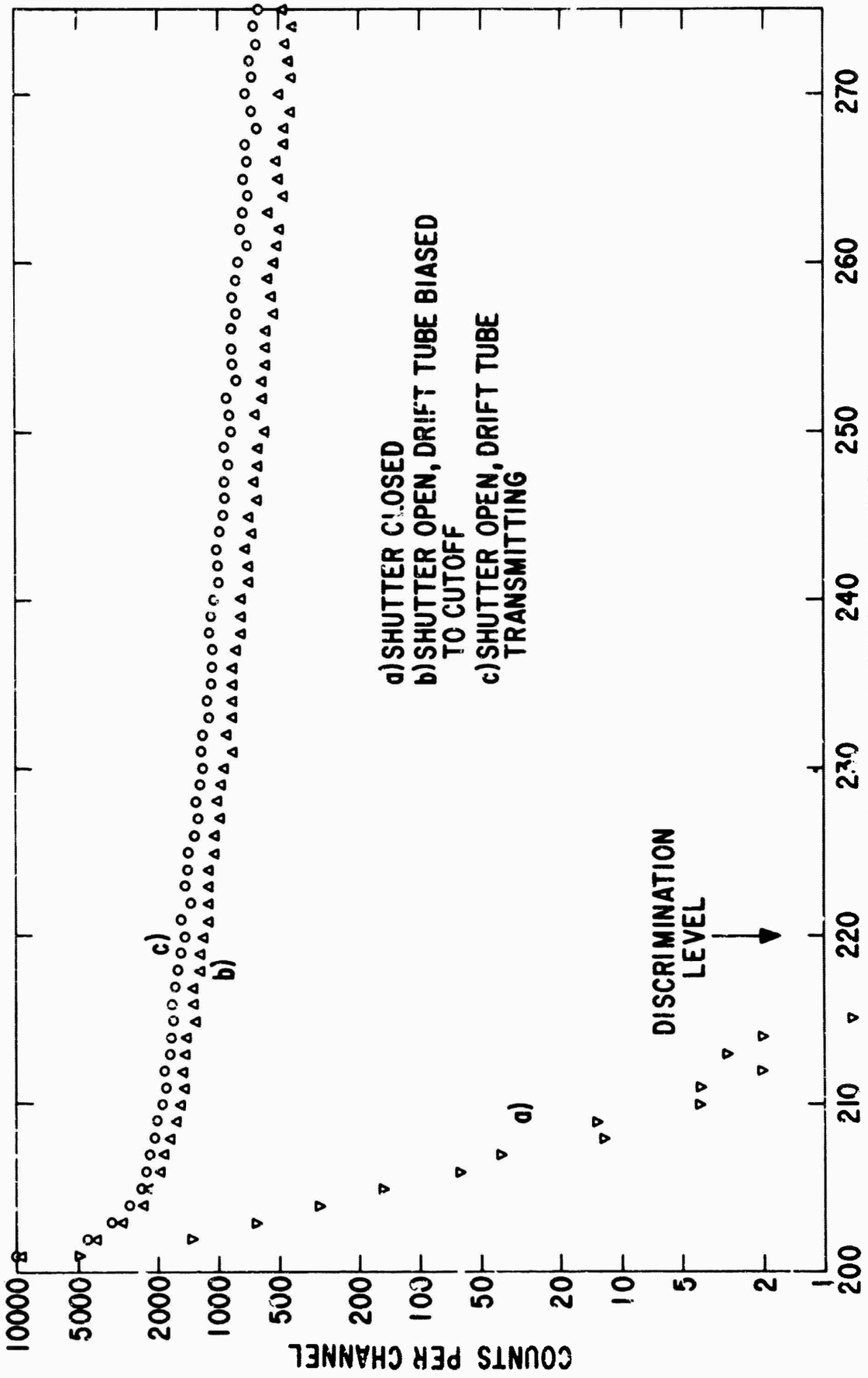

Figure 10. Distribution of detector counts according to amplitude: (a) shutter closed; (b) shutter open, drift tube biased to cutoff; (c) shutter open drift tube transmitting.

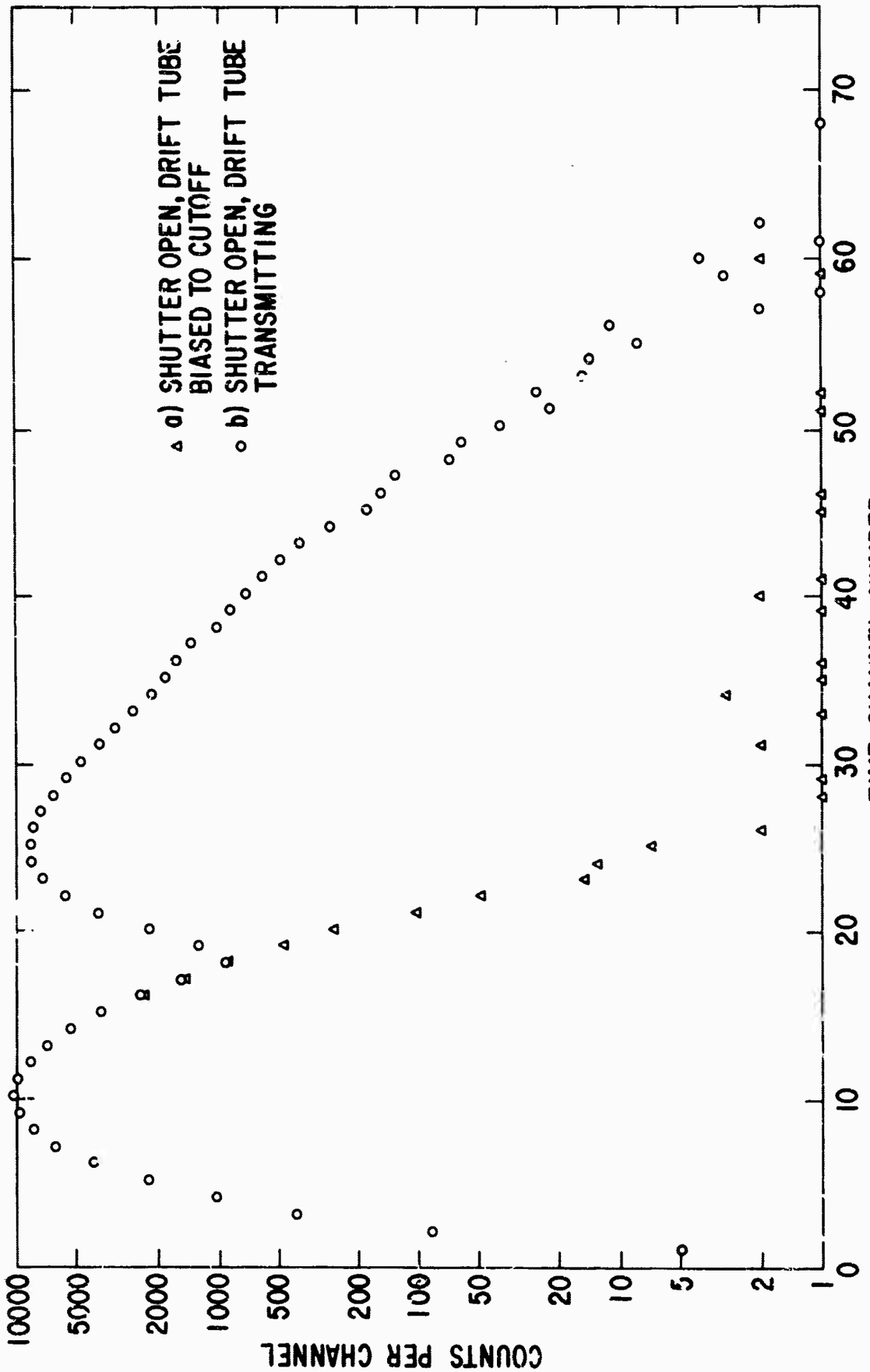

Figure 11. TOF distribution of electron counts above discrimination level: (a) drift tube biased to cutoff; (b) drift tube transmitting.

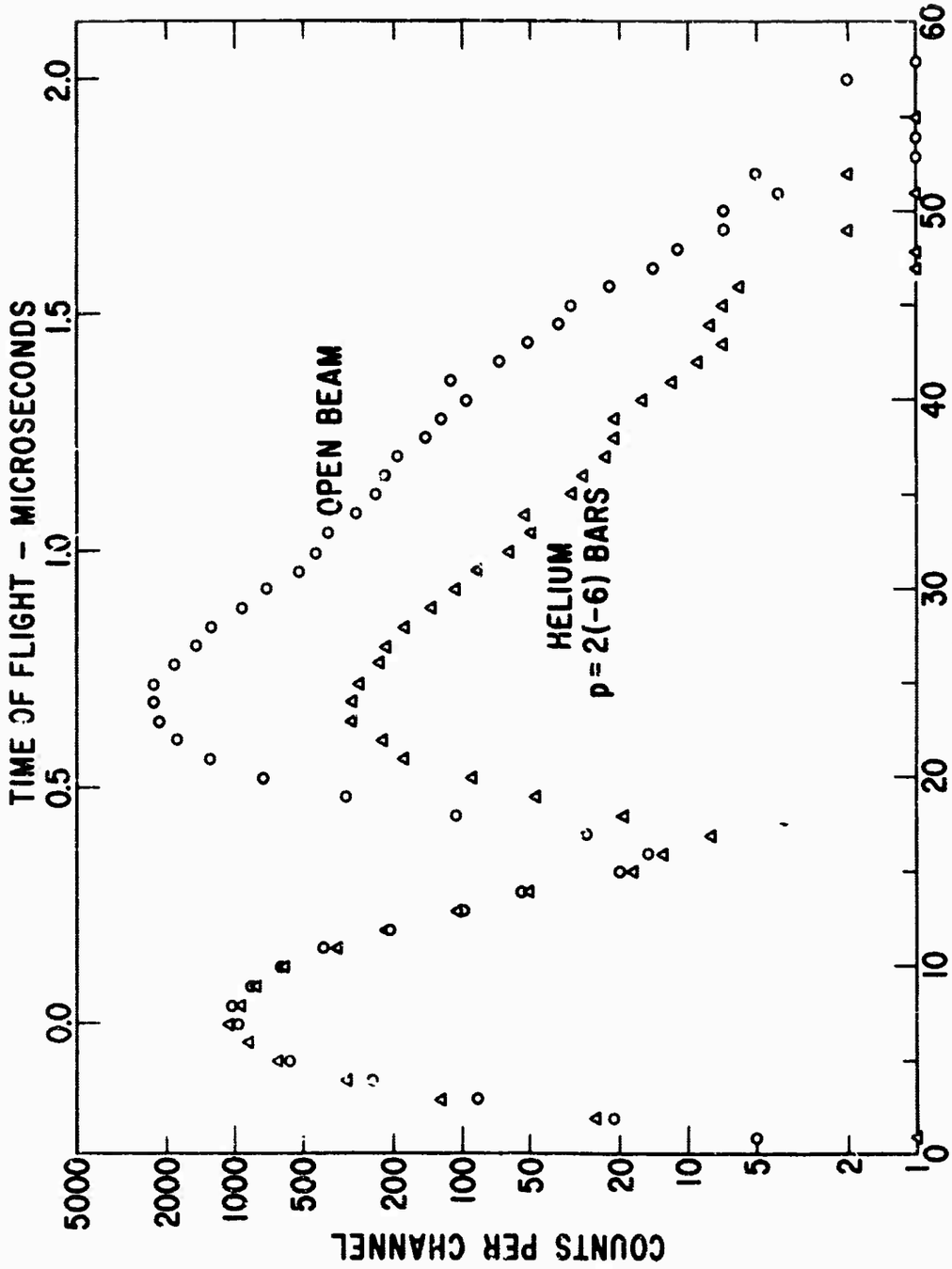

Figure 12. Comparison of TOF distributions with and without a helium specimen.

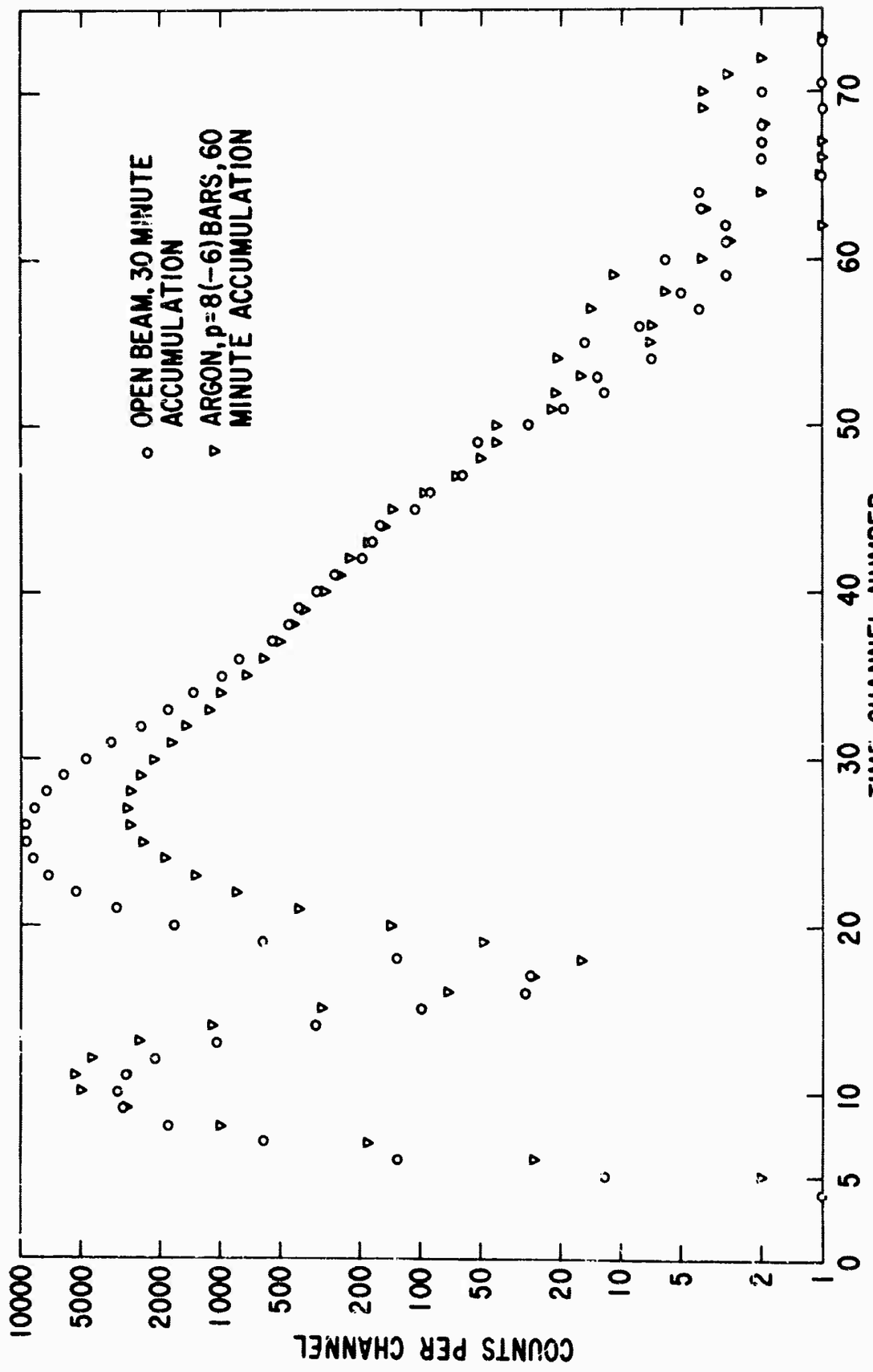

Figure 13. Comparison of TOF distributions with and without an argon specimen, at a pressure of 0.8(-5) bars.

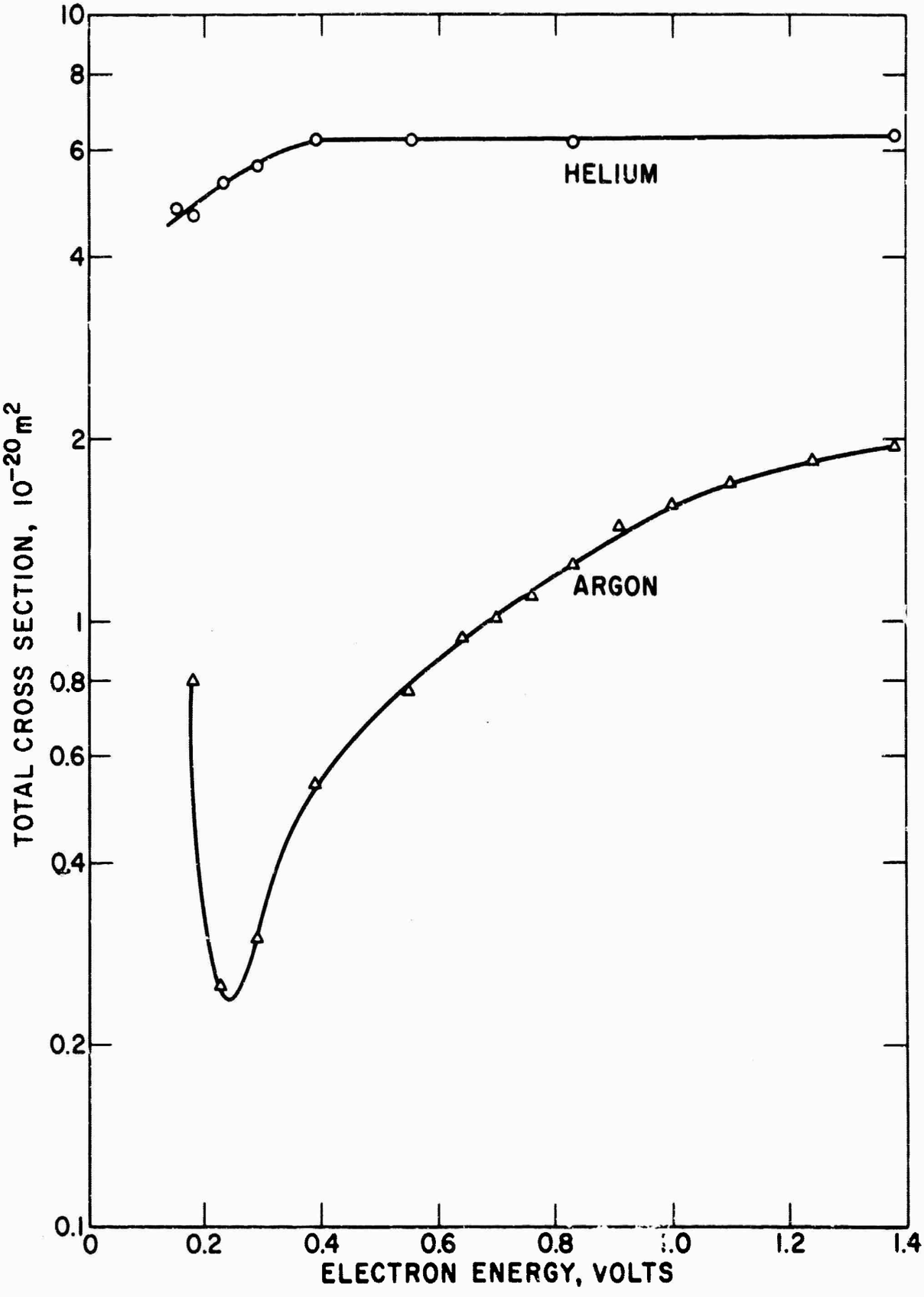

Figure 14. Preliminary measurements of total cross sections for electrons in helium and argon.

FIGURE CAPTIONS

Figure

1. Kinetic energy of an electron vs time to traverse a 0.475-meter flight path.

2. Essential electrodes and biasing requirements for TOF electron velocity selection. The electrode arrangement, diagrammed in (a), includes a baffled photoelectric source, drift tube, grid and detector. Each must be appropriately biased, as shown in (b), to establish uniform electric potential along the electron path. In (b), the dashed lines represent the respective Fermi level of each electrode.

3. Relationships of (a) integral and (b) differential energy spectrum of photoelectrons to the distribution of times of flight, (c).

4. Schematic diagram of the electron TOF spectrometer.

5. Photograph of complete electron TOF spectrometer: (1) vacuum enclosure; (2) pulsed light source; (3) lens-window; (4) emitter-baffle-electrometer; (5) drift region enclosure; (6) detector- pre-amplifier enclosure; (7) monitoring and calibration apparatus; (8) multichannel analyzer and readout units; (9) plotter; (10) punched tape readout; (11) typewriter readout; (12) biasing potentiometers; (13) specimen pressure manometers.

6. Pulsed light source and lens-window. The spark can be seen in the reflecting mirror.

7. Closeup of the spectrometer with housings and insulation partially removed, showing: (1) light source; (2) emitter-baffle flange; (3) electrometer preamplifier; (4) heating tape; (5) detector; (6) preamplifier.

8. The slat grid: (a) geometry; (b) electric potential between adjacent slats; (c) trajectory of an electron passing through the grid.

9. Calibration of the multichannel amplitude and time analyzer.

10. Distribution of detector counts according to amplitude: (a) shutter closed; (b) shutter open, drift tube biased to cutoff; (c) shutter open drift tube transmitting.

11. TOF distribution of electron counts above discrimination level: (a) drift tube biased to cutoff; (b) drift tube transmitting.

12. Comparison of TOF distributions with and without a helium specimen.

13. Comparison of TOF distributions with and without an argon specimen, at a pressure of 0.8(-5) bars.

14. Preliminary measurements of total cross sections for electrons in helium and argon.